Calibration and Implementation of Robot for Detection of X-rays

Björn Bring

LUND
UNIVERSITY

Department of Automatic Control

MSc Thesis
TFRT-6050
ISSN 0280-5316

Department of Automatic Control
Lund University
Box 118
SE-221 00 LUND
Sweden

Printed in Sweden by Tryckeriet i E-huset
Lund 2018

Abstract

While industrial robots have traditionally been designed for tasks such as pick-and-place that require a high repeatability, an increasing demand for off-line control and high-precision applications have in recent decades put higher demands on the accuracy of robots. One application in that vain is the detection of X-rays that have been scattered from a sample during X-ray diffraction, which produces interference peaks of very well-defined angles. To that end, a robot has been installed at the MAX IV synchrotron facility with the intention of having it maneuvering an X-ray detector, and the aim of this thesis is thus to improve the pose accuracy of the robot to a level that is feasible for conducting such experiments.

The robot's kinematics is calibrated through means of an optical CMM, and the joint characteristics such as backlash, friction, and joint stiffness are identified by performing a clamping routine, where the robot's end-effector is rigidly fixed to the environment. Furthermore, the calibrated model is implemented off-line in order to facilitate the control of the robot by means of the spherical coordinates that are commonly used in X-ray diffraction.

The results show that the calibrated model achieved an accuracy of 180 μm, which is close to the anticipated value of 150 μm. This means that the robot is ready to be taken into operation, even though further attempts at improving the accuracy may be undertaken in the future.

Acknowledgements

This master thesis would not have been the same without the assistance of Cognibotics AB, who provided me with the test equipment and expertise for the calibration, which I am most grateful for. I would also like to lend a special thanks to Tommy Olofsson, who with an admirable patience was willing to answer all my questions and served as a practical guide throughout this master thesis.

The staff at NanoMAX, and most especially Tomaš Stankevič and Ulf Johansson, deserves to be thanked for their interested support in my work. I also want to thank the alignment team of MAX IV for their time and support in supplying me with test equipment for the verification tests.

Lastly, I want to thank Anders Robertsson for introducing me to this master thesis project and with that the subject of robotics, the interest of which has only grown in me as the time has passed.

Contents

List of Figures

List of Tables

1

Introduction

1.1 Background

The synchrotron radiation facility MAX IV in Lund generates and uses X-rays in order to probe into the microscopic structure of various materials. This is accomplished by diverting the X-rays away from the synchrotron and into a beamline, where the beam is focused onto the sample under study. To form an image of the material in 3D, the scattered radiation has to be detected at different angles around the sample. Prior to this master thesis, this was done manually by placing the X-ray detector at the right distance and angles from the sample. By instead installing an industrial robot with a detector mounted as a tool, the same task can be accomplished with much more accuracy and less labor. The experimental environment of the sample and the scattering process can be seen in Figure 1.1 and 1.2, where the intended workspace for the robot is illustrated in terms of two angles, γ and δ, as well as the radius r. The high accuracy of the robot will primarily be required for the angular coordinates γ and δ, since a displacement in the radial direction only changes the resolution of the scanned image.

1.2 Repeatability and accuracy

In evaluating a robot's precision, there are mainly two parameters that tend to be of importance: repeatability and absolute accuracy (Figure 1.3). Repeatability can be understood as the variance or spread around the average, or barycenter, of the measured poses. Therefore, a good repeatability means that the robot will reliably acquire the same pose (position and orientation) over many iterations, but it may not necessarily correspond exactly to the commanded one. Good accuracy on the other hand means that the robot's barycenter of measured poses is close to the commanded position.

Industrial robots generally come with a high level of repeatability, which reflects the requirements needed for standard usages such as palletizing. For such repetitive

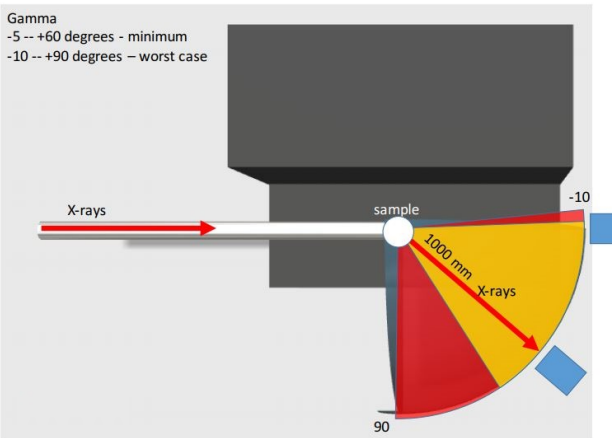

Figure 1.1 Top view of the sample environment.

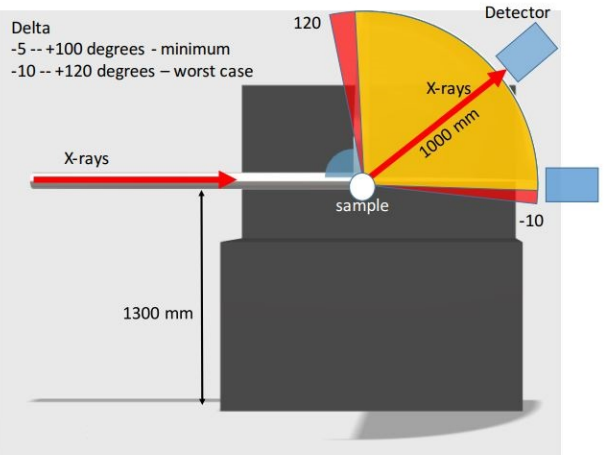

Figure 1.2 Side view of the sample environment.

tasks, it is only demanded of the robot's performance that it can be iterated many times, while the accuracy is not of very big concern. For high-precision tasks, the robots have thus commonly been in need of calibration to ascertain a better accuracy.

For on-line uses of an industrial robot, the accuracy is not very important, since the poses of the robot can be taught manually. However, if the robot is to be controlled off-line from an external PC, it is of paramount importance that the real

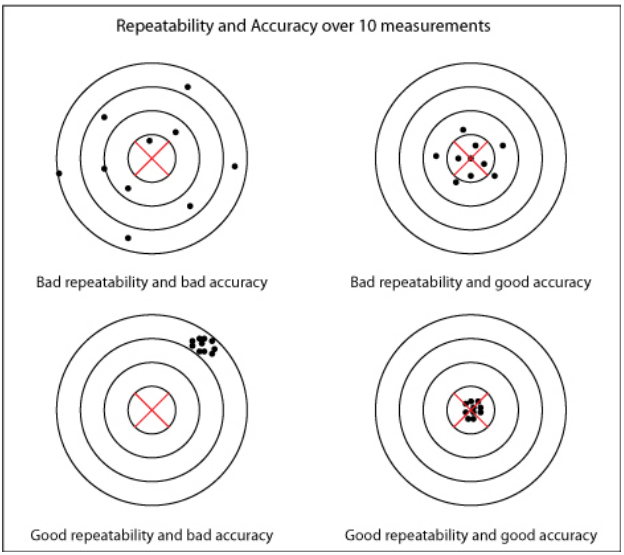

Figure 1.3 Illustration of repeatability and accuracy [**Bouchard**; **2014**].

robot's accuracy is sufficiently good [**Mooring et al.**; **1993**]. Thus, the task remains to calibrate the real robot to better replicate the behavior of the nominal off-line robot. When calibrating robots, there are several levels of calibration that can be carried out [**Mooring et al.**; **1993**]:

- Level 1: This level is commonly called "joint level calibration", with the goal being to determine the relationship between the joint transducer signal and the actual joint displacement. With this information, calibration of the joint sensors can be done.

- Level 2: This is the kinematic calibration, where the geometrical parameters that describe the robot's individual joints and links are optimized to more accurately correspond to the real robot.

- Level 3: This is the dynamic calibration, where phenomena such as backlash, friction and joint stiffness are identified and corrected for. In the event that the robot is to be controlled dynamically, a correction of the dynamic model is also included here.

In this thesis, calibration will be done on level 2 and 3.

1.3 Problem formulation

The purpose of this thesis is to calibrate the robot to as high pose accuracy as possible - ideally to match the pixel size of the detector at 55 μm - and also to implement the calibrated robot model off-line in such a way that the robot can be easily maneuvered along the desired sphere given the spherical coordinates of γ, δ, and r. The calibration procedure will be divided into two steps that each concern different parts of the robot manipulator: firstly, measurements and identification of dynamic factors such as friction, backlash and joint stiffness, and secondly, measurement and identification of the kinematic model.

Although the position of the sample will have to be calibrated in relation to the robot base coordinate frame for the robot to perform adequately, this procedure will only be mentioned shortly in the chapter "Ongoing and Future work", since it necessarily has to be done after the yearly shutdown of MAX IV, which would go beyond the time constraint of this thesis.

1.4 Previous work

The theory of robot calibration has remained almost the same for several decades, and thus the calibration methods that are commonly used have been so for a long time. The changes that have occurred have mainly been in the accuracy of the calibration devices. The majority of methods utilize an external measurement system to identify the position and orientation of the robot's end-effector, such as multi-laser tracking interferometers or 3D cameras.

Nubiola and Bonev [**Nubiola and Bonev**; **2013**] used a laser tracker to identify 34 parameters of an ABB IRB 1600 robot; 20 kinematic parameters for joint 2 to 6, 4 parameters for the joint compliances, 6 for the robot base frame, and 4 for the nonlinearity of joint 6. To validate their kinematic model, they measured as many as 1000 robot configurations in the robot's joint space, with eight spherically mounted reflectors, SMRs, on their end-effector. However, the conclusion they drew from the results was that the benefit of using more than three SMRs is negligible. With their identification of kinematic model together with a model of the joint compliances, they were able to reduce the mean/maximum position errors from 0.968 mm/2.158 mm to 0.364 mm/0.696 mm.

Another method of calibration was done by Ginani and Motta [**Ginani et al.**; **2011**], who by use of a ITG ROMER measurement arm (accuracy of 0.087 mm) managed to reduce the position errors of an ABB IRB2000 from 1.5 mm to 0.3 mm.

When calibrating the dynamics of an industrial robot, such as its stiffness and backlash, it is common that an external measurement device such as a measurement arm is used to find the deflection of the end-effector's tool center point (TCP) as a load is applied, while a force/torque sensor mounted on the wrist is used to mea-

sure the end-effector's force/torque. Instances of this can be seen in [**Wang et al.**; **2009**]. This method and similar ones rely on the accuracy of the measuring device, but one way to circumvent this dependency is to use a calibration method that fixes the robot's end-effector rigidly to the environment. This is exactly what the so called clamping method aims at remedying. The original paper that introduced the method was by Bennett et al., [**Bennet et al.**; **1992**], where it was used to calibrate the kinematic model. Since then the method has been extended to identification of dynamic parameters, as by [**Lehmann et al.**; **2013**], where joint stiffness, friction, and backlash are identified for two industrial robots. Cognibotics, which is a spin-off company from the robot research of Lund University, is a startup company that has been developing this approach.

1.5 Report outline

In structuring this report, the aim was to have it follow the procedure of calibration as best as possible, with an ensuing section of discussion about the results and methods adopted.

1. **Modeling of kinematics and dynamics** - Introduction to the theory of kinematics and dynamics of a robot manipulator.
2. **Experiments** - Description of the experimental setup and measurements for the calibration.
3. **Parameter identification** - Considerations regarding methods used for identification are mentioned here.
4. **Implementation** - Description of how the new model is implemented.
5. **Verification** - The method and results of the verification test are presented.
6. **Discussion and Conclusion** - The obtained results and chosen methods are discussed, as well as potential improvements and error sources in the measurements.
7. **Ongoing and Future work** - Ideas about how the performance of the robot can be improved further.
8. **Appendix** - Robot descriptions and other data are shown here.

2

Modeling of kinematics and dynamics

Of the total inaccuracy of the robot, the part that can be attributed to errors in the kinematic model is predominant [**Joubair**; **2014**], even more so for uncalibrated robots. The underlying causes for these errors are the manufacturing and assembly tolerances of the individual links, as well as the orthogonality and parallelism of the joint axes. These can to some degree be remedied by more precise machining of the parts, but generally at a cost that renders it unfeasible. Instead, it is common practice to use lower tolerances for the design of the robot, and then to correct the kinematic model in the control software to better emulate the real robot, which is the essence of robot calibration [**Mooring et al.**; **1993**]. For the studied robot, of model KUKA KR20R1810 C4, such a calibration has already been done by the manufacturer, and can be enabled by an option called absolute accuracy, which claims a pose accuracy of $\pm$ 500 μm and a pose repeatability (unidirectional) of 40 μm.

2.1 Forward kinematics

The process of kinematic calibration involves identification and adjustment of the kinematic parameters of the robot, which are used to describe the displacement and orientation of each of the robot's joint to its predecessor. Thus, for each joint of the robot, a reference frame is assigned which follows along with the motion of the joint; linearly for a prismatic joint, and rotationally for a revolute joint. The kinematic parameters can then be used to transform a point in one reference frame to another. For instance, the tool center point (TCP) of the end-effector can by means of the forward kinematics be expressed in the robot's base coordinate frame, which allows for much easier programming of tasks. The way that points in one reference frame is transformed to another is accomplished by so called homogeneous transformations, denoted as H_i^j, where i refers to the old frame, and j to the new frame. The transformation can be easily understood as a combination of a rotation matrix and a displacement vector. See the Appendix for further elaboration on this topic.

As an initial assumption, one might think that six parameters are necessary for each frame to fully describe the next frame - three for the displacement, and three for the rotation. This is not necessarily the case, as several methods have been designed for assigning kinematic parameters that lower the amount of parameters, at the cost of putting constraints on the way the frames are set up. In considering what kinematic model one should use, it is of benefit to review what criteria it should satisfy to be deemed appropriate for calibration. These criteria were proposed by Everett et al., [**Mooring et al.**; **1993**] and are: completeness, proportionality, and equivalence.

Completeness means that the model has sufficiently many parameters to describe the robot manipulator, and also to describe any possible configuration that the robot can achieve. The number of parameters that are required for this will of course vary depending on the robot, but a general formula can be given that only takes into account the number of revolute and prismatic joints.

$$N = 4R + 2P + 6$$

where N is the number of parameters, R is the number of revolute joints, and P the number of prismatic joints. Thus it can be concluded that for a 6 DOF articulated robot such as the one studied in this report, a total of 30 parameters is needed for the kinematic model to be complete. However, the six extra parameters included in the formula refer to an arbitrary assignment of the tool frame, and since that is not included in the calibration process, the number of parameters is reduced to 24.

A model is called proportional if a change in the robot structure corresponds to a proportional modification of the parameters. For instance, a change in the relative orientation between two consecutive joints ought to be translated into a proportional change in the parameters that describe the robot. This property is especially important during the identification process, because if the parameters vary widely, this will cause numerical difficulties and maybe even make it impossible to correctly identify model parameters.

Equivalence means that the identified parameters of the model can be translated into parameters of another kinematic model. If a model is complete, it follows that it is also equivalent, which implies that the accuracy of the robot will not depend on which type of modeling that is used.

Denavit-Hartenberg convention

The Denavit-Hartenberg convention (DH) was developed in 1955 by Jacques Denavit and Richard Hartenberg as one of the earliest attempts to standardize the kinematic modeling of spatial linkages. The convention relies on the common normal between a joint *i-1* and the succeeding joint *i* to derive four parameters which describe the coordinate transformation from frame *i-1* to frame *i*. The parameters are depicted in Figure 2.1 and are defined as:

- Joint angle θ_i: This is the rotation about the z_{i-1}-axis so as to align the x_{i-1}-axis with the x_i-axis.
- Link offset d_i: This is the distance along the z_{i-1}-axis from the origin of the *i-1*-frame to the common perpendicular x_i.
- Link length a_i: This is defined as the distance along the common perpendicular x_i from the *i-1*-frame to the *i*-frame.
- Link twist α_i: This is the rotation about the common perpendicular x_i so that the two z-axes are aligned.

Notice that for revolute joints, the joint angle is a variable and not a constant to be determined, although a small offset may be added to model a potential offset in the joint encoders.

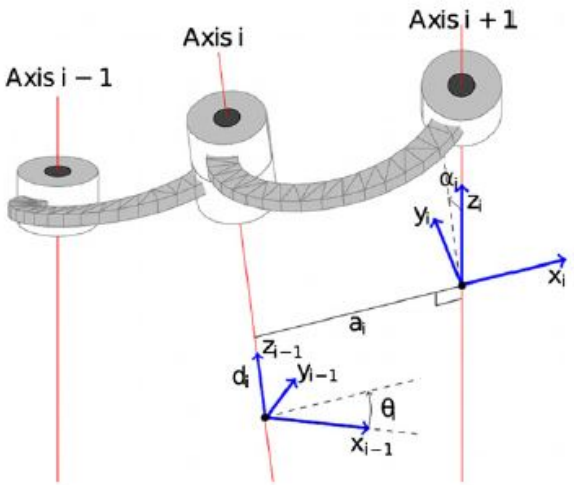

Figure 2.1 Definition of DH parameters [**Khodaygan et al.**; **2015**].

In order for this schematic to work, there are two additional rules that must be followed when setting up the DH-parameters, and they are:

- The x_i-axis must intersect with the z_{i-1}-axis.
- The y-axis for each frame is chosen so as to satisfy the right-hand rule.

By imposing these rules regarding the orientation of the axes, the amount of parameters that are required is reduced from six to four, but this also opens up the possibility of many different sets of DH-parameters, all equally valid. Another drawback

with the DH convention is that if two consecutive joints are not exactly parallel, but instead have a slight inclination, then the two z-axes of the joints may have a common normal at a point far away from the robot. Since the origin of the reference frames are set up where the two z-axes have their common normal, this will lead to dramatic changes in the parameters (more specifically the link offset d) for only slight changes of the link twist α. This disproportionality of the DH convention can pose a serious difficulty in the identification process since it leads to convergence problems for the optimization algorithms.

Modified DH convention

As a way of overcoming this difficulty, an extended or modified DH convention was proposed in 1985 by Hayati and Mirmirani [**Hayati et al.**; **1985**] that instead places the origin of frame O_{i-1} on axis *i-1*. Furthermore, another rotational parameter β has to be added (Figure 2.2). This extension of the standard DH convention where an additional parameter is included, should not be confused with the case where the standard DH convention is used but with a different labeling of the indices.

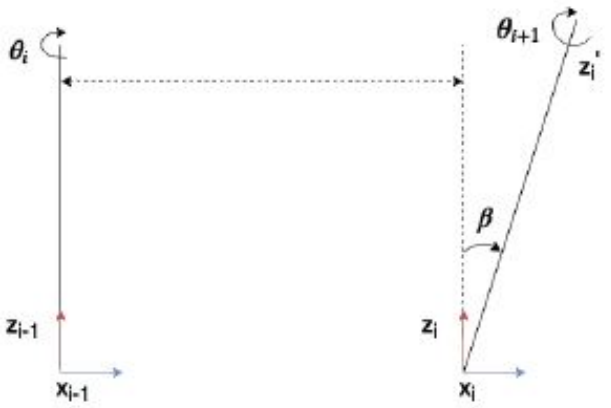

Figure 2.2 Definition of modified DH parameters.

Screw theory

Other approaches to kinematic modeling which are less common but have some advantages over the DH convention are ones based on screw theory. These apply the geometric concepts of screws to model the robot, since they embody both translation and rotation along a common screw axis. The procedure of obtaining a kinematic model using the screw theory requires a fixed coordinate frame at which the screws will be expressed, and also a reference configuration of the robot, from which each

successive screw displacement is determined. These features make it much easier to identify the kinematic parameters, and also has the benefit of having the joint variables correspond to the actual joint displacements, which is not always the case for DH convention. The one drawback with screw theory is that it is not a minimal representation of the robot manipulator [**Rocha et al.**; **2011**].

2.2 Dynamic errors

The importance of dynamic or non-kinematic factors on the accuracy of the robot can be understood by first considering which of the kinematic parameters that affect the pose repeatability. After the individual links have been machined and assembled to form the robot manipulator, their dimensions will remain constant throughout operation, given that the temperature and beam deflections from load are not changing drastically. The only kinematic parameters that vary are the joint angles θ, and the robot's repeatability can therefore be explained almost exclusively by the variation or repeatability of the joint actuators [**Shiakolas et al.**; **2015**]. The fundamental reason behind this lack of repeatability of the joint actuators is that the rotary encoders are mounted on the motor side of the joint, and in the transmission to the arm side of the joint, various effects such as friction, backlash and joint deflection creep in. Since these error sources account for the repeatability of the robot, their contribution to the accuracy is in the same proportion which the repeatability is to the accuracy - roughly 10 % [**Renders et al.**; **1991**]. For reasons of visualization, a comprehensive model of a prismatic joint can be seen in Figure 2.3

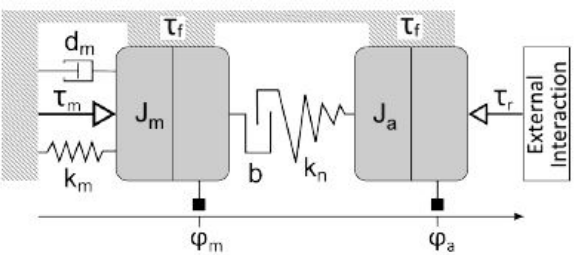

Figure 2.3 Model of a prismatic joint [**Lehmann et al.**; **2013**].

where the parameters and variables are defined as

τ_m: Torque supplied from controller to motor
τ_r: Torque exerted by gravitation or clamping fixture
φ_m: Joint angle on motor side
φ_a: Joint angle on arm side
b: Backlash
k_n: Nonlinear spring constant
τ_f: Friction torque
J_m: Actuator/Motor inertia
J_a: Arm side inertia
k_m: Stiffness accomplished by controller
d_m: Damping accomplished by controller

In view of the application that the robot is intended for, which demands high accuracy but with no need for high velocities or path tracing, the effect of inertia can be neglected without any significant impact on the end result. The dynamic effects that are identified and compensated for in the robot under study will be expanded upon in the following paragraphs.

Backlash

When two or more gears are mated, there is commonly introduced a clearance between the respective teeth of the gears, called backlash. This is necessary to account for lubrication and thermal expansion of the gears during operation, but has the downside of losing some of the mechanical motion each time the gears reverse direction. The technical definition of backlash is: "maximum distance or angle any part of a mechanical system may move before exerting appreciable force to another part." [**Bagad**; **2009**], (Figure 2.5). Thus the backlash of a joint in a robot manipulator can be characterized as the interval where the motor torque yields no rotation of the arm. In an ideal case, this would look like in Figure 2.4, [**Lehmann et al.**; **2013**] where τ_m is the motor torque, φ_m is the joint angle on the motor side, and b is the backlash.

Friction

As for any contacting surfaces, the joints also give rise to friction whenever they are actuated, both on the motor side and the arm side. There are various more or less complex models for friction that for instance include what is called Stribeck friction for low velocities [**Bittencourt et al.**; **2010**] (Figure 2.6), but in this thesis, it is modeled as consisting of only Coulomb and viscous friction. Coulomb friction is the constant force exerted regardless of angular velocity, whereas the viscous friction is proportional to the velocity.

Joint stiffness

Joint stiffness is the relationship between the applied torque and the associated angular rotation. For reasons that are evident, this relationship should ideally be linear,

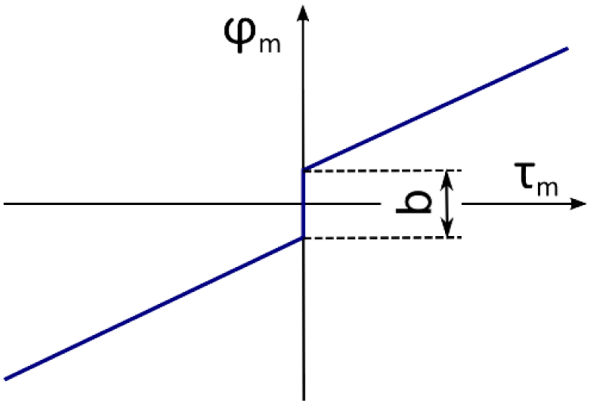

Figure 2.4 Definition of backlash [**Lehmann et al.**; **2013**].

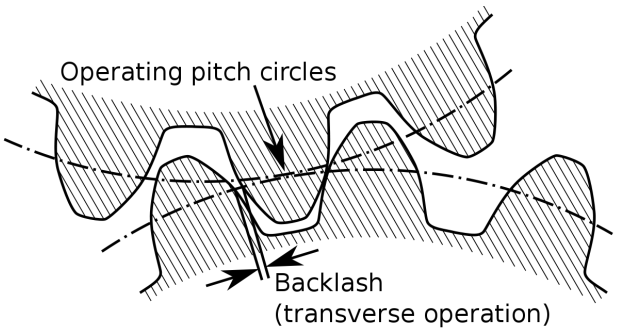

Figure 2.5 Backlash is the smallest clearance between two teeth [**Backlash**].

but in reality it usually exhibits nonlinear effects. However, for small torques, this relationship can still be approximated as being linear. This error source becomes important because of the deflection that the robot manipulator is subject to due to the force of gravity. The weight of the robot structure and the mounted tool will exert torques on each of the joints of the robot, and depending of the configuration of the manipulator, this torque will vary. For instance, if the robot arm is fully extended in the horizontal plane, the torque on the second axis - the "shoulder" of the robot - will be much greater, than if the arm is curled up with the end-effector close to the axis. For a linear approximation of the joint stiffness, the motors of each joint can thus be modeled as having torsional springs.

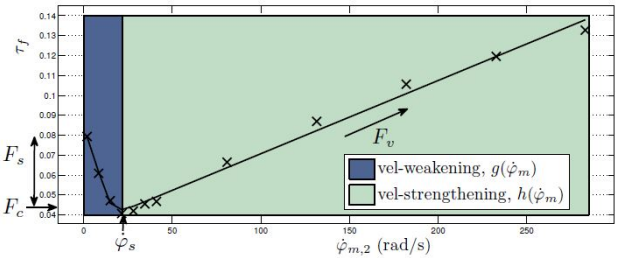

Figure 2.6 Friction definition which includes the Stribeck effect [**Bittencourt et al.**; **2010**].

3

Experiments

The experiments performed in this thesis can be described in three parts: firstly, a test of the robot's repeatability was conducted, not to improve upon it, but to verify the specification given by the robot manufacturer. Secondly, the non-geometric effects of the robot were measured during a free-air experiment followed by a clamping routine. Thirdly, the end-effector pose of the robot was measured in a large part of the workspace to gather data for calibration of the kinematic model.

3.1 Repeatability

The first measurements of the robot's repeatability was carried out using the laser interferometer IDS3010 from Attocube, which is a one-dimensional displacement sensor with an accuracy down to 10^{-12} m and with a data acquisition bandwidth of 10 MHz. Since the interferometer can only measure in one direction at a time, the procedure adopted was different from the standard way as detailed by the international standard ISO 1998:9283 [**ISO 9283:1998**], where the robot is moved to three different positions in sequence, and where the full pose measurement is taken at the same position in each cycle, for a total of 30 cycles. In this way, it is ascertained that the robot is moving in all three Cartesian directions in between the measurements and that all the dynamic errors such as backlash are excited. However, an alternative way of doing the repeatability measurement is to simply move the robot along each of the Cartesian axes at a time, and then to aggregate the results from the three directions. This means that the displacements in x, y, and z are not referring to exactly the same point, but the effect of this deviation from the standard should be negligible, since the repeatability generally is consistent across the workspace.

During the measurement, the robot was mounted with a retro-reflector and programmed to move back and forth along the robot's x-axis, with a short pause in between. By having the robot approach the same pose in opposite directions, a rough idea about the impact of the backlash can be established. These measurements at the intermediate point were taken thirteen times.

To further establish the repeatability of the robot, another test was done at a later

time in line with the descriptions laid out in the ISO standard, but with only three cycles instead of 30. This test measured all the Cartesian values simultaneously with a coordinate measuring machine (CMM). A test was also done to measure the repeatability of the CMM by having it measure a fixed point two times with an interval of ten minutes.

3.2 Free Air experiments

Because the most important non-kinematic error source is that of joint deflection caused by the gravitational force [**Renders et al.**; **1991**] - both from the tool and the robot links - it is necessary to form a gravitational model of the robot, which details the mass and center of mass for each of the robot arms. To that end, the robot was maneuvered to a number of different configurations, during which the joint torques were logged at a frequency of 10 Hz. Since the external torque exerted on the joints in a static configuration is the cross product of the gravitational force and the lever arm, both the mass and center of mass of each link can be extracted, given an appropriate set of configurations. This program was repeated a second time at 80 % of the previous velocity for the sake of determining the friction, which can be deduced from the recorded torques and motor position.

As a prerequisite for the clamping procedure, it is also necessary to take into account the transmission matrix of the robot, which relates how the torques applied by the motors influence the actuation of the joints. Due to various cross-couplings between the different joints of the robot, it is commonly found that some joints are in fact actuated by more than one motor. In the KUKA KR20R1810 robot, there exist such cross-couplings between some of the wrist joints, as can be seen under the section "Transmission matrix" in the appendix.

In addition to the free-air experiment which was used to find the friction of each joint, another experiment was carried out which only actuated the wrist. This program was generated and designed with the transmission matrix in mind so as to excite both the motor and arm side of the fifth and sixth joints, which both have couplings with the fourth and fifth axes. By reckoning with these cross-couplings, it is possible to drive the motors of each joint while keeping the arm side still, and vice versa. In this way, it was possible to identify the friction of the fifth and sixth joint on both the motor and arm side, whereas for the other axes, the friction on the motor and arm side are indistinguishable from each other.

3.3 Clamping

To compensate for effects such as backlash and joint stiffness, a clamping procedure was performed. To find the parameters which model these effects, the robot is first rigidly fixed to a 700 kg concrete block by means of a clamping fixture, to stop the robot flange from moving (Figure 3.1).

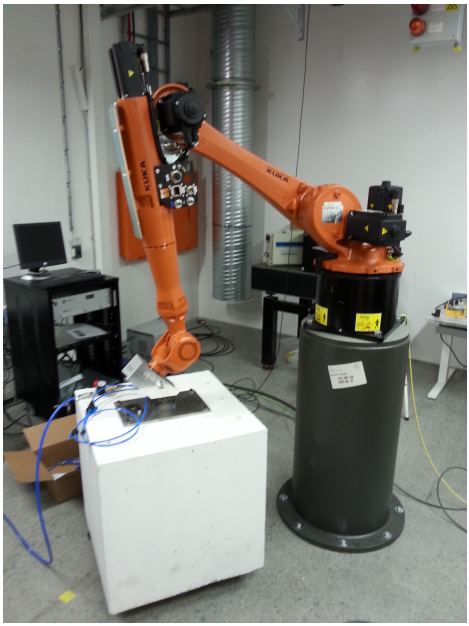

Figure 3.1 Setup during the clamping experiment.

The docking mechanism consists of three parts: a tool changer screwed onto the concrete block, a tool attachment which fits rigidly onto the tool changer, and an adapter which links the robot flange to the tool attachment. The tool attachment TA60 (Figure 3.3) is a circular device which has six tracks on the interior side, in which the balls of the TC60 (Figure 3.2) is placed. The TC60 has a matching elevation point wherein the TA60 fits. When the two are neatly mated together, compressed air is used to push a cylinder up onto the balls, whereby they are pushed into their respective tracks in the TA60. This ensures that the mounting flange of the robot will not move in either direction, or be twisted around any of the respective axes.

In designing the adapter (Figure 3.4), the 3D-CAD software SolidWorks was used. SolidWorks enables users to create 3D models where dimensions and tolerances can be specified. Apart from providing a surface for the attachment of the TA60, the adapter was also designed to serve as a mounting surface for the X-ray detector.

With the flange rigidly attached to the concrete block, the robot was first adjusted by means of incremental motions so as to find the configuration of least torque. This subsequently served as a reference position for the following measurements of backlash and stiffness. Each of the joints was then moved in turn back and forth for a total of sixteen load cases, during which the torques, joint angles, and

Figure 3.2 TC60.

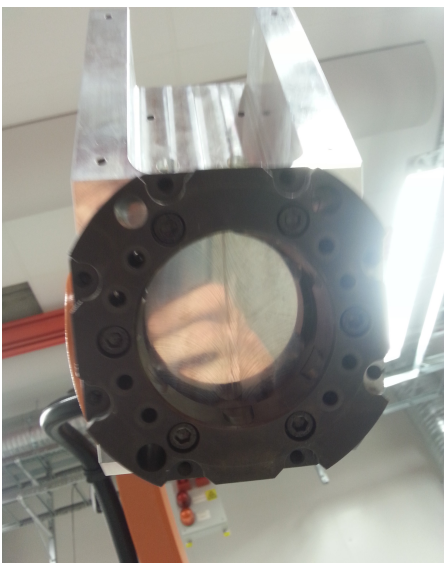

Figure 3.3 TA60.

motor angles were recorded. By plotting the motor angle against the joint torques, the characteristic backlash behavior as depicted earlier (Figure 2.4) can be seen. Unfortunately, it was discovered during the experiment that for certain of the axis movements, the concrete block was slightly displaced from the reference position due to the inadequate support the three feet of the block provided. Because of this

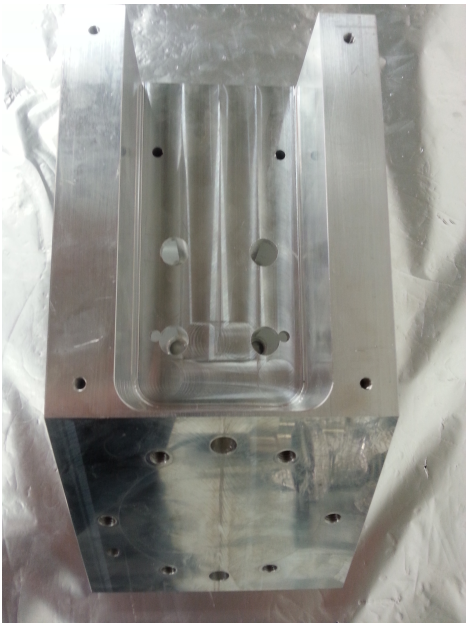

Figure 3.4 Calibration adapter.

the concrete block was later moved to a second position of more stability where the tests were repeated.

3.4 Kinematic calibration

The measurement device that was used for the data acquisition of robot poses was a Nikon camera of model Krypton K600 [**Nikon**], with an accuracy between 64 - 139 μm (Figure 3.5). Since the camera was not used at the maximum distance, the accuracy can be expected to be somewhere in the middle of the interval.

The camera consists of three infrared CCD:s that each measures the azimuthal and elevation angle of a particular LED mounted on the robot. Through means of triangulation, the Cartesian position of the LED can then be deduced in the camera's coordinate frame. The pose of the robot can through this process be obtained by using several different LEDs mounted on the tool with an accompanying stroboscopic unit that makes the LEDs flash in turn (Figure 3.6). The measured positions were chosen on a 3D grid in Cartesian space with a number of orientations for each position (with the condition that the LEDs had to be in line of sight of the camera). The kinematic solution for each pose was selected arbitrarily (elbow up or down, inverted under arm, etc.) and the configurations were sorted by joint values, so as to minimize the time consumed. This scheme was employed so as to achieve as large

Figure 3.5 Krypton K600 camera system.

spread as possible in Cartesian space as well as in joint space. Meanwhile, the joint values of the robot were logged with a sampling frequency of 10 Hz. To facilitate the subsequent data analysis, the robot was made to pause at each configuration a few seconds, which made it possible to form an average of the recorded data from both the Nikon camera and the robot.

The base frame of the robot was constructed from measurements with a touch probe on the pedestal plane and the locating elements of the base plate. This is arguably the most accurate way of finding the base frame, since it does not include any of the kinematics of the robot, but instead relies solely on the machined tolerance of the locating elements.

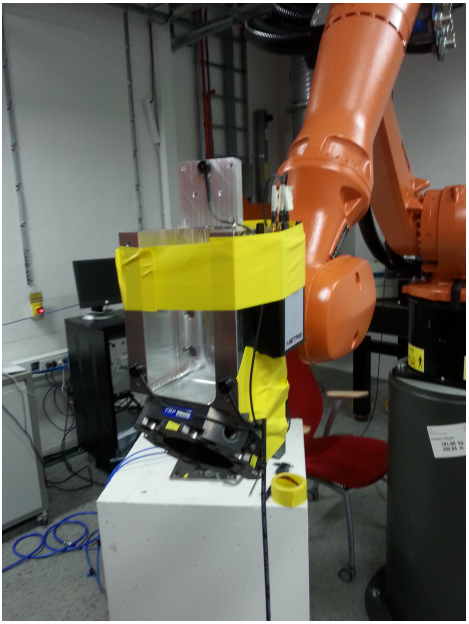

Figure 3.6 Setup with LEDs and a stroboscopic unit.

4

Parameter identification

4.1 Dynamic factors

The stiffness of each joint was modeled with torsional springs, which relate how much the motors are deflected due to external torques. For information about the result, see appendix. The friction associated with each of the joints are displayed in Figure 4.1, 4.2, and 4.3, where the last two joints incorporate friction of both the motor and arm side. With models of the friction, backlash, and joint deflection established, it is then possible to filter the measurements of the robot pose from these dynamic effects, so as to perform the kinematic calibration with joint angles that are more representative of the arm side. The kinematic parameters were first identified according to screw theory, and then converted to DH parameters.

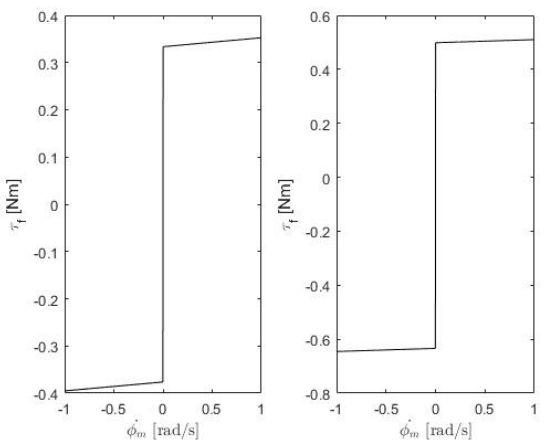

Figure 4.1 Friction of axes 1 and 2.

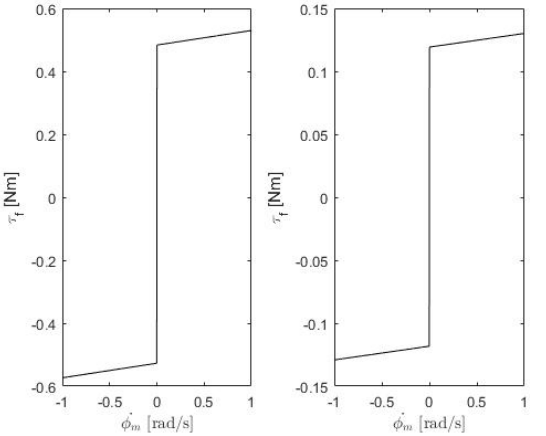

Figure 4.2 Friction of axes 3 and 4.

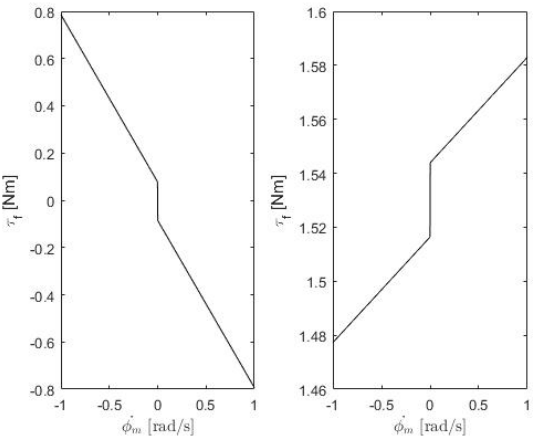

Figure 4.3 Friction of axes 5 and 6.

4.2 Optimization

When optimizing a set of parameters of a known objective function such as a kinematic model, it is important to consider what algorithm to use, as the level of convergence and robustness varies, and hence some may be more suitable than others. Common to most algorithms is that they require an initial guess of the parameters from the user, and from there on conducts an iterative search in order to minimize the objective function. For least-squares optimization, the objective function takes the form [**Nocedal**; **1999**]

$$S(\beta) = \frac{1}{2}\sum_{j=1}^{m} r_j^2(x) = \frac{1}{2}\sum_{j=1}^{m}[y_j - f(x_j,\beta)]^2 \tag{4.1}$$

where r_j is called the residual and is a function from $\mathbb{R}^n$ to $\mathbb{R}$, β is the set of parameters to be optimized, and y_j is the gathered data.

Newton's method

The Newton method is an algorithm that attempts to find a stationary point of a function ***f(x)*** by approximating it with a Taylor expansion [**Nocedal**; **1999**]. In one dimension, this means that the algorithm converges to a point x^*, where the second derivative is equal to zero, starting from an initial guess x_0. Thus, the Taylor expansion of $\boldsymbol{f}$ around the point x_n can be expressed as

$$f(x_n + \delta x) = f(x_n) + f'(x_n)\delta x + \frac{1}{2}f''(x_n)\delta x^2 \tag{4.2}$$

To find the appropriate length of the step δx that minimizes **f**, we can set the derivative of the expression with regards to δx to zero

$$0 = \frac{d}{d\delta x}\left(f(x_n) + f'(x_n)\delta x + \frac{1}{2}f''(x_n)\delta x^2\right) = f'(x_n) + f''(x_n)\delta x \implies \tag{4.3}$$

$$\delta x = -\frac{f'(x_n)}{f''(x_n)} \tag{4.4}$$

The next iteration according to the Newton method will then be

$$x_{n+1} = x_n + \delta x = x_n - \frac{f'(x_n)}{f''(x_n)} \tag{4.5}$$

For higher-dimensional problems, the derivative is replaced with the gradient and the second derivate with the Hessian matrix **H**, which consists of the second order partial derivatives.

$$x_{n+1} = x_n - [\mathbf{H}f(x_n)]^{-1}\nabla f(x_n) \tag{4.6}$$

The Newton method is not a robust algorithm and may therefore diverge, and thus requires an initial guess that is close to the minimum, but converges quadratically when close to a root [**Mathworld**].

Gauss-Newton method

As a modification of the Newton method, the Gauss-Newton method simplifies the needed computation, at the expense of less rapid convergence. Since $\mathbf{H}$ can be difficult to calculate for some problems, it is instead replaced with the matrix of first order derivatives called Jacobian $\mathbf{J}$, as in

$$x_{n+1} = x_n - [\mathbf{J}_n^T \mathbf{J}_n]^{-1} \mathbf{J}_n^T f(x_n) \tag{4.7}$$

In contrast to Newton's method, the Gauss-Newton method cannot diverge, even though it may not converge at all, even locally. The rate of converge can be slow if the initial guess is poor, but approaches quadratically when close to a minimum [**Nocedal**; **1999**].

Levenberg-Marquardt method

Another approach to finding the optimal set of parameters is to use what is called trust-region algorithms. One method that is considered to be a progenitor of this approach is the Levenberg-Marquardt method, which for each iteration approximates the function $\mathbf{f}$ as a quadratic over a trust region. At each iteration, the algorithm compares the predicted function value with the value of the objective function, and either extends or contracts the trust-region according to how well the two match. The algorithm uses the same simplification $\mathbf{H}$ as the Gauss-Newton method, with the extra variable λ which dampens the length of the next step [**Nocedal**; **1999**].

$$\left(\mathbf{J}^T \mathbf{J} + \lambda \mathbf{I}\right) \delta = \mathbf{J}^T [\mathbf{y} - \mathbf{f}(\beta)] \tag{4.8}$$

Notice that when λ approaches zero, the algorithm resembles the Gauss-Newton method, whereas if λ is large the convergence is that of steepest descent.

5

Implementation

The off-line implementation of the calibrated model was done using Python, and to operate the robot from an external PC, the add-on technology package KUKA.EthernetKRL 2.2 was used as a means to exchange data between the robot and the external PC. EthernetKRL provides a convenient way of receiving and sending data to and from the robot via a TCP/IP protocol. The coding that is required on the robot side to parse the exchanged data is minimal and straightforward.

The more challenging part of the implementation is to transfer the input from the PC to commands intelligible for the robot. The variables that are sent from the PC are the two crystallographic angles γ and δ as well as the radius from the test sample. For an illustration of the crystallographic angles, see Figure 1.1 and 1.2 in the introduction. These arguments are then to be transformed into Cartesian coordinates of the robot, and are subsequently transformed into the corresponding joint values.

5.1 Transformation into task space

The first step concerns the transformation of the spherical coordinates, γ, δ, and r, into what is called the task space of the robot. The task space consists of the Cartesian coordinates x, y, and z, as well as three Euler angles A, B, and C, which refer to rotation around the z-axis of the base frame, current y-axis, and current x-axis, in that particular order. It is by way of these coordinates that the robot is usually commanded to move, and given these values, it is then possible to construct the homogeneous transformation matrix between the base frame and the tool frame. The spherical coordinates uniquely define the position of the detector, and by converting the angles γ and δ to Euler angles, the homogeneous transformation matrix takes the following form (C is always set to zero since it corresponds to a rotation around the axis that goes through the detector area and the test sample, and does therefore not influence the position of the detector).

$$H_0^6 = \begin{bmatrix} \cos A \cos B & -\sin A & \cos A \sin B & X \\ \sin A \cos B & \cos A & \sin A \sin B & Y \\ -\sin B & 0 & \cos B & Z \\ 0 & 0 & 0 & 1 \end{bmatrix}$$

5.2 Inverse kinematics

With the homogeneous transformation matrix constructed, it is possible to solve the reverse process of forward kinematics, called inverse kinematics. Inverse kinematics is thus the problem of finding which joint angles that are the solution to a given pose of the robot. A little consideration will make it clear that there generally exist several set of joint angles that correspond to a particular pose; for instance, the robot manipulator can in many cases achieve the same pose with its elbow facing either up or down. Because of this, care must be taken to select the solution that is most suitable for the application.

For the solution of the inverse kinematic problem, both an analytic and a numeric method was used. The analytic method utilized the nominal kinematic model in order to get a rough estimate of the solution, after which the numeric solution was used to correct the estimate according to the calibrated kinematic model.

Analytic form

The benefit of using an analytic method is that it provides an exact solution according to the model that is used, contrary to numerical methods that can converge to a localized minimum. The redundancy of solutions that is generally the case for analytic methods will mainly present a problem when the robot is moving close to the robot base, where it must be ensured that the fourth and fifth axes do not rotate too much at the same time, as the tool can then easily be crashed into the base. One way of solving this is to have the sign of the fifth axis always be positive, and let the fourth axis rotate freely.

The analytic method is based on trigonometry in conjunction with knowledge of the robot structure. For instance, the first joint angle corresponds to the angle that the wrist of the robot makes with the default position of the wrist as viewed from the top, whereas the second and third joint angles can be derived from the law of cosines, since the distances between the wrist, the second joint, and the third joint are known. For the remaining joint angles, the analytic solution relies on the premise that the wrist is spherical, i.e. that the axes of rotation for axis four through six all intersect at the wrist. This makes the joint angles suitable to be modeled as three Euler angles, and since the orientation of the tool as well as the third joint can be known, the relative rotation from the third joint to the tool is sufficient to extract these Euler angles. However, because this condition of a spherical wrist was

violated for the calibrated kinematic model, it was necessary to apply a numeric method.

Numerical form

The algorithm that was used for the numeric method was the Levenberg-Marquardt algorithm as mentioned before, with the joint angles obtained from the analytic solution forming an initial guess. In this particular case, the cost functions was chosen as the deviations from the coordinates in the task space, that is X, Y, and Z according to the homogeneous transformation matrix seen above, as well as four of the elements of the rotation matrix (the convergence of the solver was not affected by which entries were chosen).

5.3 Implementation of dynamic effects

In the kinematic calibration, the measurements of the poses were filtered from the dynamic effects in order to improve the identification, but to implement these effects off-line is connected with some difficulties. As the robot is moved to a commanded position, it is hard to estimate where in the backlash each of the joints are at the outset of the motion, and thus how much of it that should be filtered. This is different from when the joints have to reverse motion, since then the whole backlash has to be traversed. A similar problem is seen with regard to the friction, since it is dependent on how much the joints are actuated during the motion to the commanded position, and also the angular velocity. The one effect that is constant (at a given configuration) regardless of the trajectory of the robot is the joint deflections caused by the robot's and the tool's weight, which also takes up the predominant part of what causes the inaccuracy. The implementation of the joint deflections was provided by Cognibotics, and the exact algorithm remains undisclosed.

6

Verification

The test that was conducted with the robot using the laser interferometer from Attocube showed a bidirectional (one-dimensional) repeatability of 11.24 μm, the result of which can be seen in Figure 6.1 and 6.2. As a comparison, the unidirectional repeatability test along the same direction showed a repeatability on the order of 3-5 μm. Equivalent measurements along the y and z-axes have as of yet not been done, since the repeatability tests were only carried out to ascertain that the specification given by the robot manufacturer at 40 μm was reasonable. The result of measuring the repeatability of the robot using the Nikon camera can be seen in Figure 6.3, which yielded a repeatability of 26 μm. The same figure also shows the average accuracy to be about 150 μm for these five poses. To measure the repeatability of the Nikon camera itself, two measurements series were carried out on a fixed point, where averages were formed from a total of 14000 samples, acquired with a frequency of 500 Hz. This resulted in a repeatability of 10.4 μm. To validate the

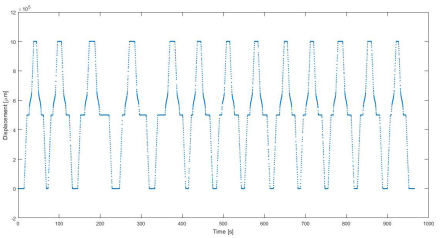

Figure 6.1 Displacement along the x-axis with a pause in between the end points.

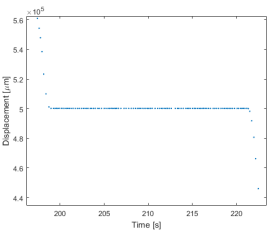

Figure 6.2 Zoomed in portion of an intermediate point

obtained robot model, a verification was conducted that compared the absolute accuracy model of the robot with the calibrated model. To make the verification more adapted to the intended application, the robot was moved on a grid which spanned an eighth of a sphere similar to the actual sample environment, (Figure 6.4). One benefit of doing the verification on a sphere is that the measured errors can then be

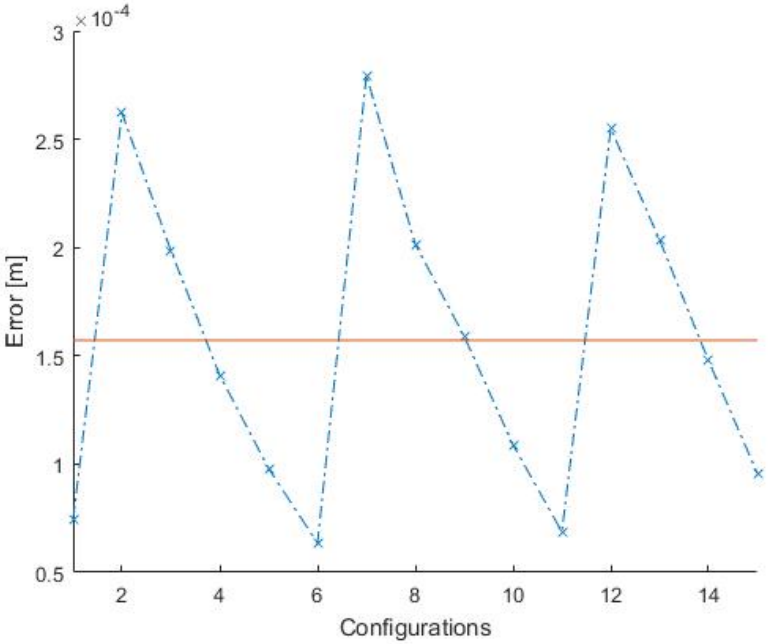

Figure 6.3 Aggregated Cartesian error for three cycles of five points in an inclined plane.

separated into errors in the radial direction as well as errors along the surface of the sphere, which will provide useful information in regards to the experiments.

Unfortunately, the sphere had to be placed away from the workspace that will later be used for the experiments, in order for the measurement camera, a Leica Absolute Tracker AT402, to have unobstructed vision of the robot (Figure 6.5). This tracker measures the azimuthal and elevation angles as well as the distance to its target, which can later be converted into Cartesian coordinates in an appropriate frame, in this case the base frame of the robot.

The program consisted of 78 configurations, at which three positions were measured using a spherical mounting reflector (SMR) on the fiducial points of the mounting plate numbered from one to three (Figure 6.6).

By the time of these validation measurements, the robot had been transported to its final position (previously it had been installed to a place where the cell was more spacious) and aligned with the use of locating pins. This made it impossible to use a touch probe to measure the pin holes with, and subsequently to construct the base frame that way. Instead, the first and second axes were moved each in turn tracing a half circle, while the end-effector was measured at ten equidistant positions. From these measurements, a circle could be fitted in the software program of Leica, called

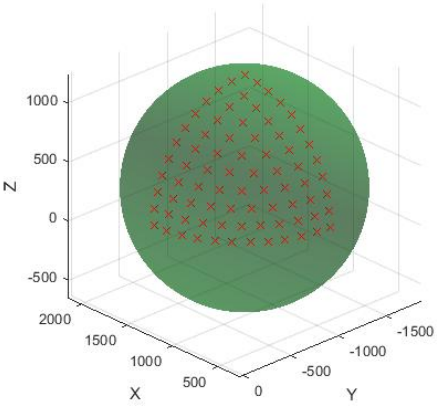

Figure 6.4 Verification sphere with programmed points.

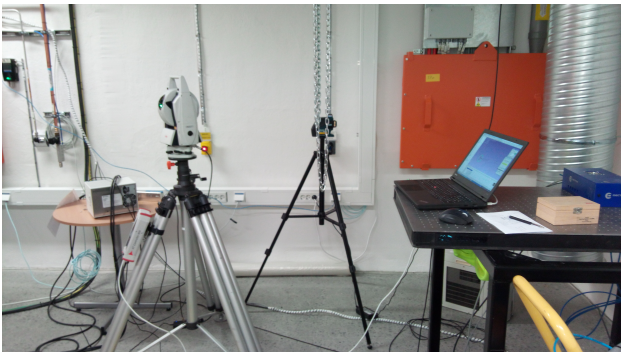

Figure 6.5 Leica Absolute Tracker AT402

Spatial Analyzer, as well as the normal of the constructed circle. Having thus measured the two axes of rotation for axis one and two, it was then possible to find the common normal between the axes. Given this projection of the second axis onto the first axis, it was then possible to transform the gathered data from that coordinate frame to the one used as base frame for the kinematic calibration.

Due to restricted possibilities of the software Spatial Analyzer to group measurements of different fiducial points, it was reckoned that measuring all three fiducial points in sequence at all the 78 configurations would be too time consuming, and it was instead decided that the program would be run three times in a row, each time measuring a different fiducial point. This implies that the repeatability of the robot and the camera are then affecting the fitting of the fiducial points to the

Figure 6.6 Mounting plate with the fiducial points numbered 1 to 3 used.

end-effector, but since the repeatability had been found to be on the order of ten to twenty microns, it was deemed acceptable for the accuracy.

On first analyzing the measurements of the laser camera, it was concluded that the calibrated model did not bring an improvement to the accuracy as compared to the absolute accuracy model, as can be seen in Figure 6.7 and 6.8. This large discrepancy was later found to originate from an error in the implementation of the calibrated model, which rendered the calculated joint deflections much too big due to a redundant conversion from radians to degrees. Moreover, the compensation did not account for the robot's own weight, only the mass of the tool. Although this makes the results useless for comparison with the absolute accuracy model of the robot, or for direct verification of the calibration, it can still be used as a sort of reference. If the errors in the implementation are corrected for and the model is working as intended, it should be able to predict the measured error, given the same joint values as was used during the verification. The predicted error was calculated by applying the forward kinematics of the corrected model on the joint values supplied to the robot during the verification, and subtracting from that the poses obtained from the corrected model's joint values. Both of these sets of joint values correspond to the robot's pose before any joint deflection has been accounted for, and can be seen in Figure 6.9. If the corrected model is assumed to estimate the joint deflections accurately, then the measured error, which includes the deflections, should match the

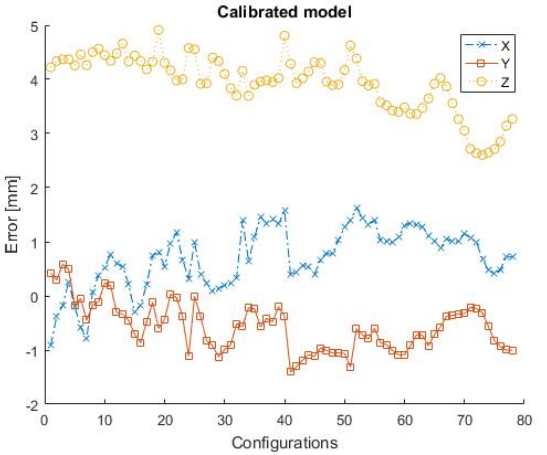

Figure 6.7 Measured error of the calibrated model.

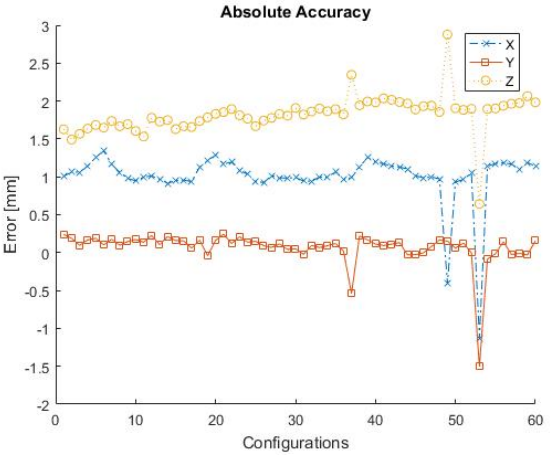

Figure 6.8 Measured error of the absolute accuracy model

predicted error. This, however, was not reflected in the obtained results, as seen in Figure 6.10.

Based on the unsatisfying results of both the absolute accuracy and calibrated model, another verification test was planned with the Nikon camera that was used before, where the calibration of the base frame followed more along the lines of how it was done during the calibration. Although the locating pins were inserted, one of the pin holes was still available to be measured by the touch probe, and the

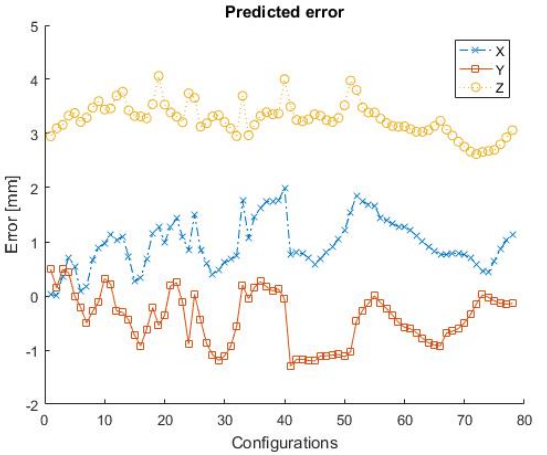

Figure 6.9 Predicted error of the calibrated model.

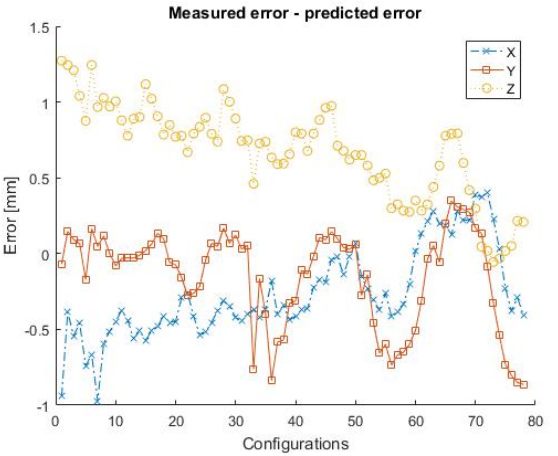

Figure 6.10 The predicted error subtracted from the measured error.

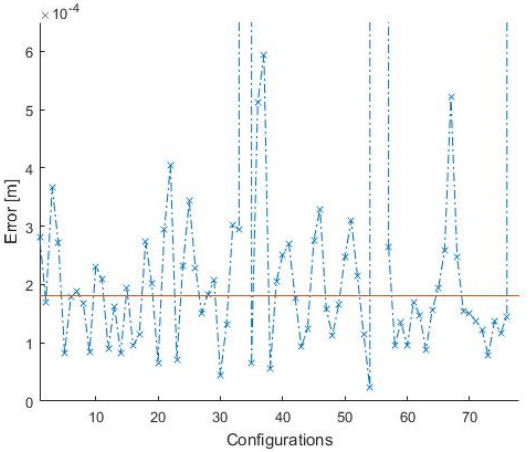

Figure 6.11 Cartesian error for the final verification, with the average marked in red.

base calibration could thus be improvised by measuring the pedestal plane, one of the locating elements, as well as the rim of the base plate. This is a much more crude way of measuring the base frame, since the tolerance of the base plate is not as high as for the locating elements, but this procedure still resembles the one used during calibration more than the one adopted with the Leica camera. The idea with this is that if the obtained error of the two models can be attributed to a faulty measurement of the base frame, that difference will be made more evident with the results of the second verification test. Furthermore, a series of test of the accuracy according to the ISO standard was carried out, which entails that the robot is moved in a sequence of five points, and with the pose measured in each cycle, for a total of five cycles. This method reduces the influence of the repeatability, in contrast to the verification tests that were performed on the sphere with the Nikon camera, where the robot is only moved to a configuration once.

The result of this new validation can be seen in Figure 6.11, with an average accuracy of 181 μm. In fact, this measurement shows the validation performed using an implementation of Cognibotics instead of my own implementation, since access to the robot was prohibited by the time errors in the code had been fixed. However, subsequent to this validation test a comparison between the joint angles for the different implementations was done, and the angles obtained through my implementation agreed with those of Cognibotics to an order of 10^{-6} rad or less, which for a fully extended robot arm translates to a positional error for axis one of approximately 2×10^{-6} m, which is negligible in the context of the experiments that the robot will be used for.

7

Discussion and Conclusion

7.1 Interpretation of results

The differences in methodology of how the base frame was measured during the verification as opposed to the calibration procedure can possibly account for much of the error that is seen in Figure 6.8, especially the error in z. From the deflections observed during the verification process, it can be noted that they are on the order of 1 mm, which would have an effect on the accuracy of the base frame measurement. As the second axis was moved on an arc tracing a half circle, it is safe to assume that the end-effector must have been deflected in the negative z-direction, perhaps as much as 1 mm. The overall effect of this is that the axis of rotation of the second axis (which corresponds to the upper arm) is displaced in the negative z-direction, which in turn would displace the base frame by the same amount. Given the circumstances at the time, with the locating pins inserted, it was considered best to proceed with the idea of moving axes 1 and 2 to construct the base frame. However, an alternative method that would bypass this problem would have been to use LEDs glued directly onto the links of the robot, as the deflections would then not alter the shape of the traced circle or translate it in any direction. Another point of improvement regarding the measurement would be to have the three fiducial points measured at the same time, since the fitting of the end-effector to the gathered data would then not be influenced by the robot's repeatability. The effect of this is limited to less than 40 μm, but for a verification test that attempts to assert an accuracy of about 150 μm, this constitutes a significant part.

By a simple inspection of measured error of the absolute accuracy model, it can be seen that the variance in all three Cartesian directions is small with the exception of outliers, but that the mean value along especially the x- and z-axis are rather significant. This is another indication of that the base frame as measured during the verification is different to the one used by the absolute accuracy model. It is unlikely that such an offset could be caused by a poor modeling of the kinematic model, since the spatial errors that each of the links contribute with will either be accumulated or canceled, depending of the configuration. Since each of the links can be thought of as a rigid body, the magnitude of the errors in position and ori-

entation from one joint to the succeeding one due to errors in the kinematic model will be constant, but with varying direction according to the joint angle. Therefore, it is expected that for a set of configurations where the joint angles vary considerably as in the verification test, any modeling error of the kinematics will yield an increase in variance, but not an offset, especially not of the magnitude seen in the aforementioned plots.

One last thing that may have an impact on the inaccuracy of the absolute accuracy model is that the setup steps laid out by the robot manufacturer have not been followed all the way through. The manufacturer advises the operators to perform an initial mastering of the robot when it is first commissioned - which means that the mechanical and electrical joint angles are aligned - but also to master it again when the tool is loaded, in order to account for the slight change in motor offset that is induced by the load. However, this effect will most likely be insignificant since the load is so small. Another theory is that the mastering performed with a load is only to have a reference in the event that the robot needs to be remastered after service, in which case a potentially heavy load will not have to be dismounted. If this is true, the mastering with a load mounted would not make a difference at all.

That the predicted error of the calibrated model did not match the measured error is harder to explain through means of a poorly measured base frame, as the variance is much more significant than for the absolute accuracy model. Plausible reasons for this discrepancy could be that the joint deflections are still not calculated accurately enough, even though the pattern of the predicted error somewhat resembles the measured error. Another explanation could be that the kinematic model of the calibration is inadequate in representing the real robot. Both of these causes are reasonable, though difficult to either corroborate or discard without further measurement data. One supposition that is taken for granted in this comparison of measured error and predicted error is that the joint deflections of the robot are equal for configurations that are a few millimeters apart, especially in the z-direction. This is of course an approximation, and shows that the method is inferior to a verification with a working model.

The accuracy of roughly 150 to 180 μm that can be seen in the final verification tests (Figures 6.3 and 6.11) is on the level that could be anticipated from the chosen calibration method. An interesting difference between these two results is that the first is derived from measuring five positions three times, whereas the second result is obtained from a much more varied set of poses, but with only one measurement for each pose. This means that the first measurement accounts for the repeatability to a greater degree, while the second maybe gives a more appropriate picture of the accuracy in the whole workspace.

One surprising result is that the repeatability of the Nikon camera and the robot as measured by the said camera turned out to differ by only 16 μm. The natural conclusion would then be that the difference is caused by the repeatability of the robot, but since the measurement of the robot was only carried out for three cycles, as opposed to 30 which is the custom, this result ought rather to be seen as an es-

timate. Nevertheless, it is evident that the repeatability is better than the specified value of 40 μm, quite possibly as low as 20 μm. One effect that may contribute to the repeatability of the robot is the Coulomb friction associated with the arm side. Since the torques generated on the arm side are not corrected for by the servo controller of the robot, this means that any torque applied on the motor side must be greater than a certain threshold to initiate any motion. Due to the small angles which the arms make in order to exceed the threshold, the resulting deviation of the end-effector (or end of the link) can be approximated as the deviation the lever arm makes when displaced by this angle (since the displacement is almost exclusively orthogonal to the lever arm, the deviation can be estimated as the sine times the lever arm). The necessary torque on the motor side to overcome the threshold can be obtained through the transmission matrix of the robot, see appendix. Taking the fifth axis as an example, the Coulomb friction on the arm side was found to be 8 Nm. With a lever arm of 153 mm, and a motor stiffness of 1.28 Nm/rad, the maximum deviation caused by the Coulomb friction is calculated as

$$153\text{mm} \cdot \sin(((8.03\text{Nm} \cdot -0.01381254)/1.28\text{Nm/rad}) \cdot -0.01381254) = 183.2\mu m$$

However, there are several complications involved in the interpretation of this equation, one being that it assumes the joint is of a stick-slip model, which means that the arm remains motionless until the torque exceeds the Coulomb threshold, whereupon it is moved in a discrete step, see figure 2.5. In actuality, the arm will move in a continuous manner as soon as the threshold is overcome, and the actual deviation will be smaller than what is given in the right-hand side. Another thing which most certainly is not accurate is the unusually low value of the spring constant. This is probably due to the fact that the fixture that was used during the clamping procedure was not sufficiently stable. Furthermore, since the free-air experiments were done at low speeds, this meant that uncertainty in the estimation of the friction would inevitably be introduced.

7.2 Methodology

The question of what metrology method and test equipment that is most suitable for such a calibration as this one is another point of important consideration. As the desired accuracy of the robot is 55 μm, corresponding to one pixel of the X-ray detector, selecting a coordinate-measuring machine (CMM) with an accuracy of 90 μm is of course to abandon that goal as realistic to achieve. As a comparison, the international standard ISO 9283:1998(en), which details performance criteria and test methods, advocate that the total measurement error does not exceed 25 % of the characteristic that is being tested [**ISO 9283:1998**]. Although this is certainly a valid remark, there are few available test equipments with an accuracy of that level. In addition, the robot manufacturer estimated that the accuracy of the robot could be reduced to approximately 100 μm, which compared to the preliminary and

anticipated accuracy of 150 μm is rather close.

During the measurements it became apparent that the way in which the real time data of the Nikon camera was recorded was not working without problem. Up to this thesis work, this has been done using a UDP transmission, but this time the data turned out to be faulty with regards to the geometry of the touch probe. Instead, the software of the camera was downgraded and conventional TCP was used.

8

Ongoing and Future work

One fundamental drawback with the servo control of the robot is that it only gets feedback from the rotary encoders on the motor shafts of the joints, and not any feedback from the actual pose, which is the variable that is of true interest. One way of closing the loop in this regard is to install a laser tracker in the robot cell, which would continuously measure the pose of the robot in relation to the robot base and apply the necessary compensation in the task space. This will come with a few practical difficulties in that it must be ensured that the tracker can measure the tool as well as the base for any configuration. In the sample environment that is intended for experiments, it is doubtful if there is any such place where the laser tracker could be installed and fulfill these requirements. It remains an open question whether the NanoMAX team wishes to pursue this solution or anything of similar sort, or if they are content with the accuracy as it is. This would potentially improve the accuracy, but this setup would at the same time be fraught with inaccuracies of its own, such as the inaccuracy of the tracker itself, the interface to the control system, and the mechanical bandwidth of the manipulator, which limits the response of the force control.

In the implementation of the calibrated model, there is an option of specifying the joint velocities and joint accelerations for any movement, in order for the model to compensate for friction. Because the commanded positions that are sent from the external PC will be specific to the particular experiment that is being conducted, this makes it difficult to include any effect that friction may have on the accuracy. One way of remedying this would be to have an intermediate point which the robot returns to before any commanded pose is being initiated by the robot. In this way, it is ensured that the robot always approaches a given pose in the same direction, thus improving the repeatability. This however may only be feasible for some types of experiments, since other will require the detector to move between two positions in a short time span. Thus it will depend on how fast the robot can move if this approach is a viable or not.

Given that the robot is calibrated to sufficient degree, it remains a task to have the test sample stage calibrated in the base frame of the robot. Since all the commanded poses will have this point as their origin (the midpoint of the sphere), it

is essential that it is calibrated accurately. Fortunately, there is a straightforward and possibly very accurate method for doing this; as the X-ray beam is incident on a crystal lattice, it will be reflected on successive atomic planes and interfere either constructively or destructively. Under conditions where they interfere constructively, called Bragg diffraction, the angles of incidence follow the formula [**Bragg**]

$$m\lambda = 2d\sin\theta \tag{8.1}$$

where λ is the wavelength of the X-ray beam, m is an integer, d is the separation of atomic planes, and θ is the angle of incidence. Because the wavelength of the X-ray beam can be tuned with very high precision, and the separation d is also very well defined, this means that the angles of incidence, and in turn the scattering angles, will be well defined. By then recording the Cartesian position as the detector finds several of these intensity peaks, the point of scattering can be deduced through trigonometry. The accuracy of this test sample calibration will naturally be limited by the accuracy of the robot.

9

Appendix

Homogeneous transformation

The homogeneous transformation from the 0-frame to the 1-frame is given by

$$H_0^1 = \begin{bmatrix} (x_1^0)_x & (y_1^0)_x & (z_1^0)_x & (o_1^0)_x \\ (x_1^0)_y & (y_1^0)_y & (z_1^0)_y & (o_1^0)_y \\ (x_1^0)_z & (y_1^0)_z & (z_1^0)_z & (o_1^0)_z \\ 0 & 0 & 0 & 1 \end{bmatrix} = \begin{bmatrix} R_0^1 & o_0^1 \\ 0_{1x3} & 1 \end{bmatrix}$$

where R_0^1 is a rotation matrix and o_0^1 is a displacement vector. The last row is only added for sake of formalism. By applying these transformations consecutively in the right order to a point in the tool frame, the same point can be represented in the robot base frame.

The KUKA KR20R1810 robot is a 6 DOF articulated robot, with the nominal kinematic model represented in the DH convention in Table 9.1.

Table 9.1 DH-parameters of the nominal robot

	θ [rad]	d [m]	a [m]	α [rad]
Link 1	$-\theta_1$	-0.520	0.160	$-\pi/2$
Link 2	θ_2	0	0.780	0
Link 3	$\theta_3-\pi/2$	0	0.150	$\pi/2$
Link 4	θ_4	-0.860	0	$-\pi/2$
Link 5	θ_5	0	0	$\pi/2$
Link 6	θ_6	-0.153	0	0

Joint stiffness

The spring constants describe the stiffness of each motor, see Table 9.2.

Table 9.2 Spring constants

Axes	1	2	3	4	5	6
Spring constants [Nm/rad]	9.92	14.18	18.66	2.07	1.28	0.56

Transmission matrix

The transmission matrix T is used to convert joint angles to motor angles in the form of $\theta_{motor} = \mathrm{T}\theta_{joint}$, and vice versa, as well as for other related properties, such as torque and angular velocity. Notice that the fifth and sixth joint exhibit cross-couplings with the fourth and fifth axes.

$$T = \begin{bmatrix} 7/880 & 0 & 0 & 0 & 0 & 0 \\ 0 & 26/4345 & 0 & 0 & 0 & 0 \\ 0 & 0 & 1/117 & 0 & 0 & 0 \\ 0 & 0 & 0 & 37/2940 & -37/162540 & -161292583/607130785800 \\ 0 & 0 & 0 & 0 & -98/7095 & -1127/3512025 \\ 0 & 0 & 0 & 0 & 0 & 368/17787 \end{bmatrix}$$

Bibliography

[1] Planetary Gearbox Glossary. *http://www.entasistr.com/en/yazar.asp?yazar=detay&id=18*. Accessed: 2017-10-31.

[2] Bagad, V. S. (2009). "Mechatronics", Technical Publications. ISBN 9788184314908, 2009.

[3] Bennett, D. J., Hollerbach, J. M., and Henri, P.D. (1992). "Kinematic Calibration by Direct Estimation of the Jacobian Matrix", Proceedings 1992 IEEE International Conference on Robotics and Automation, 12-14 May 1992, Nice, France, pp. 351-357.

[4] Bittencourt, A. C., Wernholt, E., Sander-Tavallaey, S., and Brogårdh, T. (2010). "An Extended Friction Model to capture Load and Temperature effects in Robot Joints", Proceedings of the 2010 IEEE/RSJ International Conference on Intelligent Robots and Systems, 18-22 October, 2010, Taipei, Taiwan, pp. 6161-6167.

[5] Bouchard, S. (2014). "Robotic Gripper Repeatability Definition and Measurement". *https://blog.robotiq.com/bid/36551/Robotic-Gripper-Repeatability-Definition-and-Measurement*, July 8, 2014. Accessed: 2017-11-09.

[6] "Bragg's Law and Diffraction: How waves reveal the atomic structure of crystals", *http://skuld.bmsc.washington.edu/ merritt/bc530/bragg/*. Accessed: 2017-12-12.

[7] Ginani, L. S., Motta, J. M. S. T. (2011). "Theoretical and Practical Aspects of Robot Calibration with Experimental Verification", Journal of Brazilian Society of Mechanical Sciences and Engineering, 33, pp. 15-21.

[8] Hayati, S., and Mirmirani, M. (1985). "Improving the absolute positioning accuracy of robot manipulators", Journal of Robotic Systems, 2, pp. 397-413.

[9] "Manipulating industrial robots – Performance criteria and related test methods (ISO 9283:1998, IDT)".

[10] Joubair, A. (2014). "What are the Sources of Robot Inaccuracy?", *https://blog.robotiq.com/bid/72831/What-are-the-Sources-of-Robot-Inaccuracy*, Oct 14, 2014. Accessed: 2017-12-02.

[11] Khodaygan, S., and Hafezipour, M. (2015). "Error Reduction in Spatial Robots Based on the Statistical Uncertainty Analysis", SAE Int. J. Mater. Manf. 8(2):2015, doi:10.4271/2015-01-0435, p 264.

[12] "Leica Absolute Tracker AT402", *http://metrology.leica-geosystems.com/en/Leica-Absolute-Tracker-AT402_81625.htm*. Accessed: 2017-12-03.

[13] Lehmann, C., Olofsson, B., Nilsson, C., Halbauer, M., Haage, M., Robertsson, A., Sörnmo, O., and Berger, U. (2013). "Robot Joint Modeling and Parameter Identification Using the Clamping Method", IFAC Conference on Manufacturing Modelling, Management and Control. June 19-21 2013, Saint Petersburg, Russia, pp. 813-818.

[14] "Newton's Method" *http://mathworld.wolfram.com/NewtonsMethod.html*. Accessed: 2017-12-10.

[15] Mooring, B. W., Roth, Z. S., and Driels, M. R. (1993). "Fundamentals of manipulator calibration", Automatica: The Journal of IFAC, The International Federation of Automatic Control, July 1993, 29(4), pp. 1151-1153.

[16] "K-CMM - Portable Optical CMM System", *https://www.nikonmetrology.com/en-gb/product/k-cmm*. Accessed: 2017-12-10.

[17] Nocedal, J., Wright, S. J. (2006). "Numerical Optimization", Springer-Verlag New York, Inc.

[18] Nubiola, A., Bonev, I. A. (2013). "Absolute calibration of an ABB IRB 1600 robot using a laser tracker", Robotics and Computer-Integrated Manufacturing, 29 (2013), pp 236-245.

[19] Renders, J. M., Rossignol, E., Becquet, M., and Hanus, R. (1991). "Kinematic Calibration and Geometrical Parameter Identification for Robots", IEEE Transactions on Robotics and Automation, vol 7, no 6. December 1991, pp. 721-732.

[20] Rocha, C.R., Tonetto, C.P., and Dias, A. (2011). "A comparison between the Denavit–Hartenberg and the screw-based methods used in kinematic modeling of robot manipulators", Robotics and Computer-Integrated Manufacturing, 27, pp. 723-728.

[21] Shiakolas, P. S., Conrad, K. L., and Yih, T. C. (2015). "On the Accuracy, Repeatability, and Degree of Influence of Kinematics Parameters for Industrial Robots", International Journal of Modelling and Simulation, 22:4 (2002), pp. 245-254.

[22] Wang, J., Zhang, H., and Fuhlbrigge, T. (2009). "Improving machining accuracy with robot deformation compensation", In Proc. IEEE/RSJ Int. Conf. on Intelligent Robots and Systems (IROS), St. Louis, MO, USA, 10-15 October, 2009, pp. 3826–3831.

Lund University
Department of Automatic Control
Box 118
SE-221 00 Lund Sweden

Document name
MASTER'S THESIS

Date of issue
June 2018

Document Number
TFRT-6050

Author(s)
Björn Bring

Supervisor
Ulf Johansson, MAX IV, Sweden
Anders Robertsson, Dept. of Automatic Control, Lund University, Sweden
Rolf Johansson, Dept. of Automatic Control, Lund University, Sweden (examiner)

Title and subtitle
Calibration and Implementation of Robot for Detection of X-rays

Abstract

While industrial robots have traditionally been designed for tasks such as pick-andplace that require a high repeatability, an increasing demand for off-line control and high-precision applications have in recent decades put higher demands on the accuracy of robots. One application in that vain is the detection of X-rays that have been scattered from a sample during X-ray diffraction, which produces interference peaks of very well-defined angles. To that end, a robot has been installed at the MAX IV synchrotron facility with the intention of having it maneuvering an X-ray detector, and the aim of this thesis is thus to improve the pose accuracy of the robot to a level that is feasible for conducting such experiments.

The robot's kinematics is calibrated through means of an optical CMM, and the joint characteristics such as backlash, friction, and joint stiffness are identified by performing a clamping routine, where the robot's end-effector is rigidly fixed to the environment. Furthermore, the calibrated model is implemented off-line in order to facilitate the control of the robot by means of the spherical coordinates that are commonly used in X-ray diffraction.

The results show that the calibrated model achieved an accuracy of 180 mm, which is close to the anticipated value of 150 mm. This means that the robot is ready to be taken into operation, even though further attempts at improving the accuracy may be undertaken in the future.

Keywords

Classification system and/or index terms (if any)

Supplementary bibliographical information

ISSN and key title
0280-5316

ISBN

Language
English

Number of pages
1-55

Recipient's notes

Security classification

http://www.control.lth.se/publications/